Crystal structures of lanthanide terephthalate tetrahydrate, $R_2(C_8H_4O_4)_3(H_2O)_4$, R = La–Er

Emma L. Markun, and James A. Kaduk [a)]
North Central College, 131 S. Loomis St., Naperville, IL 60540, USA

(Received 18 November 2021; accepted 31 January 2022)

The crystal structures of 11 lanthanide terephthalate tetrahydrates have been refined using laboratory X-ray powder diffraction data and optimized using density functional techniques. The lattice parameters and R–O bonds exhibit expected trends based on the cation size. The R–O bond distances in the Rietveld-refined structures are similar. However, in the density functional theory (DFT)-optimized structures, the bond distances break into two distinct groups, longer and shorter R–O bonds. This indicates that the bond distance restraints imposed upon the refined structures may have a greater impact than is expected from their weights. The aromatic carboxyl groups were not completely planar, but it is known that the carboxyl groups can rotate to accommodate hydrogen bonding and coordination to the metal. Both water molecules coordinated to the lanthanides act as hydrogen bond donors, but only one of the three unique carboxyl groups acts as an acceptor.
[doi:10.1017/S0885715622000033]

Key words: lanthanide, terephthalate, powder diffraction, Rietveld refinement, density functional theory

I. INTRODUCTION

Metal-organic frameworks (MOFs) are of current interest for their use in a variety of applications such as gas storage, gas adsorption, and use as catalysts (Furukawa *et al.*, 2013; Wang and Astruc, 2020). As such, the development of MOFs has grown to encompass the use of lanthanide metal centers in place of traditional transition metal centers to further increase their versatility. As the production of lanthanide-based MOFs continues to expand, it is important to be able to identify and characterize any dense phases which may be made as co-products or byproducts of the MOF synthesis and to have good reference patterns for these structures available to facilitate their identification.

The pattern of an attempt to prepare a porous La-MOF yielded a product a diffraction pattern of which was an excellent match to PDF entry 00-069-1206, $Dy_{0.6}Y_{1.4}(C_8H_4O_4)_3(H_2O)_2$ (Bushmarinov, 2018). This PDF entry provides a structural reference (Khudoleeva *et al.*, 2017), but no atom coordinates are provided. A search of the PDF for lanthanides and "terephth" in the name yielded entries 00-034-1984 $La_2(C_8H_4O_4)_2(H_2O)_4$ (Sherif, 1970), 00-058-0902 $Eu_2(C_8H_4O_4)(OH)_4(H_2O)_2$ (Serre *et al.*, 2002), as well as compounds containing fragments in addition to terephthalate. The experimental pattern could be indexed (DICVOL14, Louër and Boultif, 2014) on a primitive triclinic unit cell with $a = 6.2833$, $b = 10.2700$, $c = 10.3321$ Å, $\alpha = 102.374$, $\beta = 92.018$, $\gamma = 101.795°$, and $V = 635.30$ Å^3. A reduced cell search in the Cambridge Structural Database (Groom *et al.*, 2016) yielded three hits: $Nd_2(C_8H_4O_4)_3(H_2O)_4$ (AMIXOK, Zehnder *et al.*, 2011), $Ce_2(C_8H_4O_4)_3(H_2O)_4$ (CELDAA, Zhu *et al.*, 2012), and $EuTb(C_8H_4O_4)(H_2O)_4$ (EXUTAU, Grishko *et al.*, 2015). Additional connectivity and name searches yielded $Er_2(C_8H_4O_4)(H_2O)_4$ (AMIXIE, Zehnder *et al.*, 2011). Searches of the primary literature yielded Daiguebonne *et al.* (2008). Although these authors characterized a series (La through Tm) of $R_2(C_8H_4O_4)_3(H_2O)_4$ "coordination polymers", neither the atom coordinates or powder patterns have appeared in a database. It should be noted that, although there are differences in the formulation of these compounds in the literature, they are all tetrahydrates.

Thus, crystal structures of cerium, neodymium, terbium, and erbium terephthalate tetrahydrates have been published. We have undertaken to synthesize the remaining lanthanide compounds, characterize them structurally using X-ray powder diffraction techniques, and examine trends in the structures. Moreover, it was found that lanthanides smaller than Er crystallize in a different structure. These compounds will not be discussed in this paper.

II. EXPERIMENTAL

The lanthanide terephthalate tetrahydrate compounds were prepared by dissolving 1.2 mmol of the hydrated lanthanum chloride salt ($RCl_3{\cdot}xH_2O$, R = La–Er) in 15 ml of water and adding 0.3151 g (1.5 mmol) of sodium terephthalate, which was synthesized by treating 1 equivalent of terephthalic acid with 2 equivalents of sodium hydroxide in ethanol, and isolated as a white solid. After stirring for 2 h at room temperature, the lanthanide terephthalate tetrahydrate precipitate is isolated using vacuum filtration, washed with water and acetone, and allowed to dry.

The X-ray powder diffraction patterns (Figure 1) were measured on a PANalytical Empyrean Debye–Scherrer

[a)]Author to whom correspondence should be addressed. Electronic mail: kaduk@polycrystallography.com

https://doi.org/10.1017/S0885715622000033 Published online by Cambridge University Press

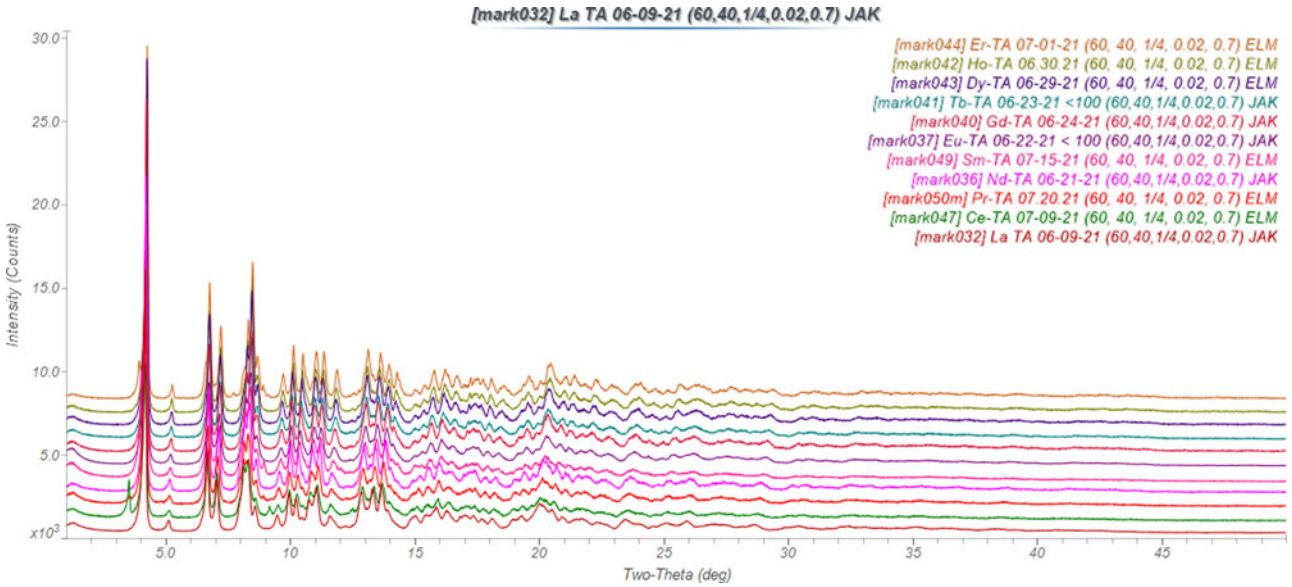

Figure 1. Powder patterns of $R_2(C_8H_4O_4)_3(H_2O)_4$ (measured using Mo K_α radiation), R = La–Er, showing that the compounds are isostructural.

diffractometer equipped with an incident-beam focusing mirror and an X'Celerator detector. The patterns (1–50° 2θ, 0.0083557° steps, 1.2 or 4 s per step, 1/4° divergence slit, 0.02 radian Soller slits) were measured from 0.7 mm diameter glass capillary specimens using Mo Kα radiation.

Rietveld refinements were carried out using GSAS-II (Toby and Von Dreele, 2013). Only the 3.0–50.0° portion of the pattern was included in the refinement (d_{min} = 0.839 Å). All C–C and C–O bond distances and angles were subjected to restraints, based on a Mercury/Mogul Geometry Check (Bruno *et al.*, 2004; Sykes *et al.*, 2011). The Mogul average and standard deviation for each quantity were used as the restraint parameters. The R–O bond distances were restrained using a distance calculated by the bond valence method and 0.05 or 0.10 Å as the standard deviation. The restraints contributed 2.2–7.3% to the final χ^2. The hydrogen atoms were included in calculated positions, which were recalculated during the refinement using Materials Studio (Dassault, 2020). The U_{iso} were grouped by chemical similarity. The U_{iso} for the H atoms were fixed at 1.3× the U_{iso} of the heavy atoms to which they are attached. Some U_{iso} for C and O refined to unreasonable values, so they were fixed at average values derived from the CELDAA structure. It was possible to refine some R anisotropically. The peak profiles were described using the generalized microstrain model, although for heavier R the data supported only refining isotropic microstrain. In general, refinements of the microstrain coefficients and the lattice parameters simultaneously were unstable, so the microstrain coefficients were fixed in the final refinements. An absorption model was included. The μR values were calculated using the tool on the 11-BM web site (https://11bm.xray.aps.anl.gov/absorb/absorb.php), assuming a 50% packing density. The values varied from 0.63 for La to 1.13 for Er. The background was modeled using a 6-term shifted Chebyshev polynomial. The final refinements yielded the residuals shown in Table I. The largest errors in the difference plots (Nd sample in Figure 2) are in the shape of the strong low-angle 010 peak.

TABLE I. Rietveld refinement residuals for $R_2(C_8H_4O_4)_3(H_2O)_4$

R	R_{wp}	GOF	# Variables	ΔF (e/Å^{-1})	% Restraints
La	0.04405	2.46	77	0.28(6) −0.25(6)	5.0
Ce	0.06206	1.77	77	0.59(9) −0.34(9)	4.1
Pr	0.06579	1.99	77	0.78(10) −0.43(10)	3.3
Nd	0.05371	1.70	82	0.29(7) −0.28(7)	7.3
Sm	0.08265	2.42	82	2.34(15) −0.60(15)	2.2
Eu	0.04256	2.41	77	0.32(7) −0.27(7)	6.8
Gd	0.05168	1.71	82	0.32(8) −0.36(8)	4.7
Tb	0.05792	1.78	77	0.67(10) −0.40(10)	4.3
Dy	0.05113	1.64	82	0.43(10) −0.39(10)	4.1
Ho	0.06690	2.03	83	0.47(10) −0.40(10)	3.1
Er	0.05136	1.60	102	0.58(8) −0.29(8)	3.4

The density functional theory (DFT) optimizations were carried out using VASP (Kresse and Furthmüller, 1996) (fixed experimental unit cell) through the MedeA graphical interface (Materials Design, 2016). The calculations were carried out on 16 2.4 GHz processors (each with 4 Gb RAM) of a 64-processor HP Proliant DL580 Generation 7 Linux cluster at North Central College. The calculations used the GGA-PBE functional, a plane wave cutoff energy of 400.0 eV, and a *k*-point spacing of 0.5 Å^{-1} leading to a 3 × 2 × 2 mesh. In general, the calculations used the default (from structure) option for magnetism. For Ce, Sm, and Eu, the spin-polarized option was used, as either the compound was a metal (Eu) or the band gap was unreasonably small in the default calculation.

https://doi.org/10.1017/S0885715622000033 Published online by Cambridge University Press

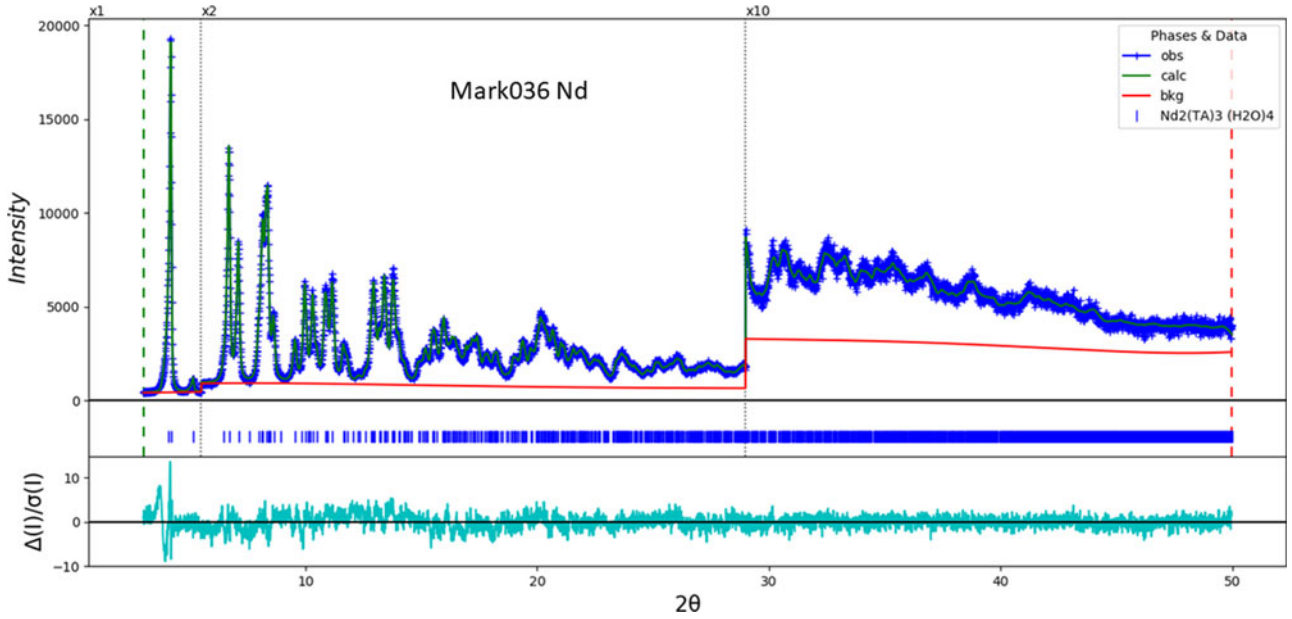

Figure 2. The Rietveld plot for the refinement of $Nd_2(C_8H_4O_4)_3(H_2O)_4$. The blue crosses represent the observed data points, and the green line is the calculated pattern. The cyan curve is the normalized error plot. The vertical scale has been multiplied by a factor of 10× for $2\theta > 29.0°$.

III. RESULTS AND DISCUSSION

All of these compounds are isostructural, as indicated by the similarity of the powder patterns (Figure 1). The root-mean-square (rms) Cartesian displacement between the 11 Rietveld-refined and VASP-optimized structures averages 0.138(41) Å, well within the normal range for correct powder structures (van de Streek and Neumann, 2014). The rms difference between the Rietveld-refined and four single crystal structures is 0.106(15) Å, and the difference between the single crystal and VASP-optimized structures is 0.070(14) Å. The largest differences tend to be at oxygen atoms. As expected (van de Streek and Neumann, 2010), the agreement between single crystal and DFT structures is better than for powder structures, though we can be confident that all of these structures are correct. A typical comparison is shown in Figure 3.

The synthesis of these lanthanide terephthalate compounds produced a dense MOF structure consisting of alternating layers of lanthanide coordination spheres and terephthalate anions parallel along the *b*-axis (Figure 4). The eight coordinate lanthanides are isolated, forming an approximate square antiprism. The isolated lanthanides are bridged by the carboxyl groups of the terephthalate anions. Each carboxyl group bridges two lanthanides, and each lanthanide is coordinated to six carboxyl O atoms and two water molecule O atoms. The water molecules are approximately *cis*. The approximate plane of both independent phenyl rings is –413.

Most of the VASP calculations were carried out in the default mode, with magnetism defined by the model. These mainly yielded semiconductor band structures, with band gaps around 2.9 eV. Ce and Eu were anomalous, with Ce yielding a very small band gap, and Eu being a metal.

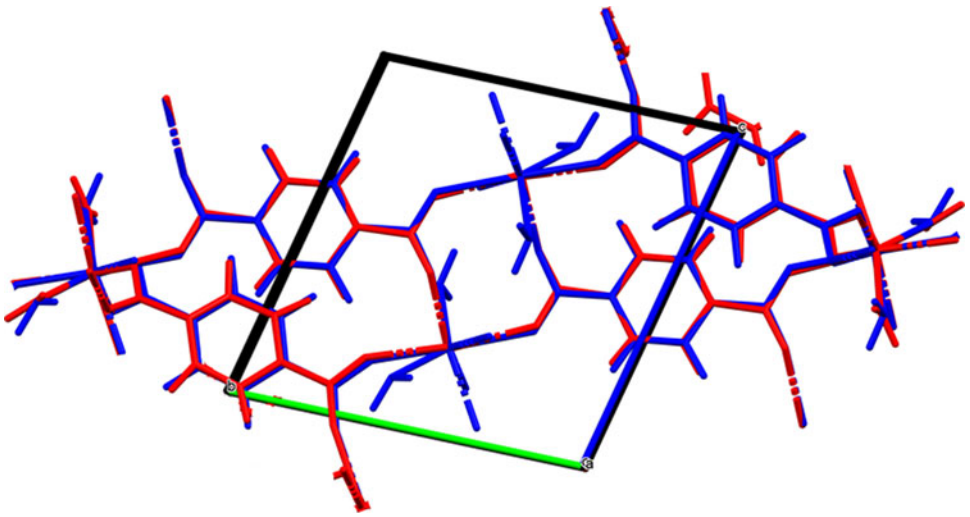

Figure 3. Comparison of the Rietveld-refined (red) and VASP-optimized (blue) structures of $Pr_2(C_8H_4O_4)_3(H_2O)_4$. The rms Cartesian displacement is 0.139 Å.

https://doi.org/10.1017/S0885715622000033 Published online by Cambridge University Press

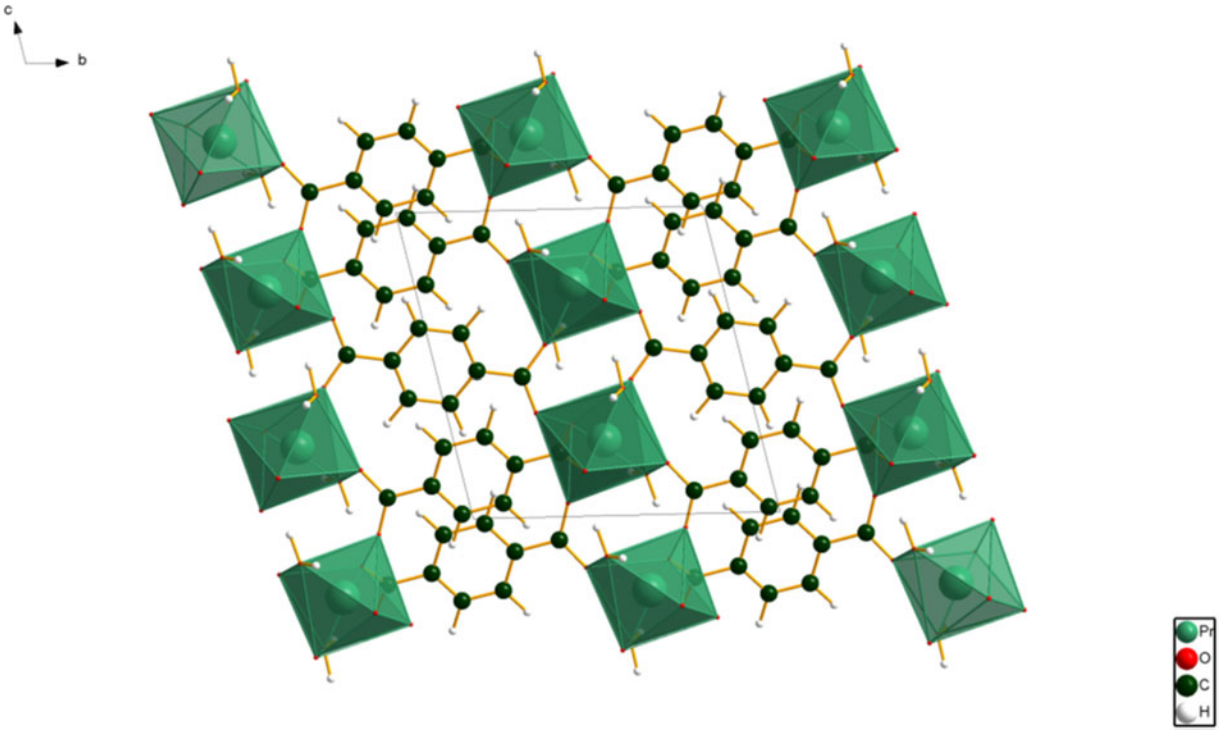

Figure 4. Crystal structure of $Pr_2(C_8H_4O_4)_3(H_2O)_4$, viewed down the *a*-axis. The oxygen atoms lie at the corners of the polyhedra and are plotted as small red dots, rather than as balls.

Spin-polarized calculations were carried out for these (as well as for Sm, which has anomalous geometry); these yielded half-metallic ferromagnets, but the geometries were identical to those from the first calculations. We can thus apparently rely on the VASP geometries, but should interpret any energetic results with caution. Conventional DFT is known to have difficulty with highly localized *f* states, and methods beyond conventional theory (such as correlated band theory, DFT + U) are required to do accurate energy calculations for lanthanides (Kozub *et al.*, 2016).

The Density of States was calculated for R = La and Ho. The highest occupied states consisted mainly of O and C *p*-states. The O *p*-states of the water molecules were slightly lower in energy. The bonding in the La and Ho compounds was similar.

We use the Shannon and Prewitt (1969) 8-coordinate ionic radii as a measure of the size of the lanthanide cations. Our lattice parameters are very similar to those reported by Daiguebonne *et al.* (2008), but measured with higher precision. The triclinic unit cell volumes exhibit an excellent linear correlation to the ionic radius (Figure 5). The least-squares fit is $V = 381.2(49) + 209.9(45)r$. Most of the individual lattice parameters exhibit similar monotonic trends, but β exhibits more interesting behavior (Figure 6). This angle is almost constant for the smaller R, but increases for the larger lanthanides, even though the overall change is very small.

Almost all of the bond distances, angles, and torsion angles fall within the normal ranges indicated by a Mercury/Mogul Geometry check (Macrae *et al.*, 2020). In the refined structures, the main unusual features occur in the carboxyl group C2–O4–O5 in the terephthalate lying on the center of symmetry (Table II). A few of the C5–C7–C11 phenyl ring angles in this terephthalate are also unusual. In the La, Nd, and Dy structures, the O1–C8–C10–C12 torsion angle is flagged as unusual. These describe the orientation of the carboxylate group which acts as hydrogen bond acceptors. The torsion angles occur on the tails of planar distributions (torsion around 0°). In the DFT-optimized structures, there are many fewer unusual features; they also occur in the carboxyl group C8–O1–O2. The agreement of the refined and optimized torsion angles is good (Figure 7). The O1–C8–C10–C12 torsion is about 25°, the O5–C1–C9–C3 is about 10°, and the O3–C2–C5–C7 is about −15°. Aromatic carboxyl groups are more flexible than is commonly believed (Kaduk *et al.*, 1998). Rotation out of the aromatic plane has a small energy cost which can easily be compensated for by the formation of hydrogen bonds. Moreover, the C–O bond which is a hydrogen bond acceptor displays unusual features.

The Rietveld-refined metal-oxygen (R–O) bond distances tend to decrease as the cation radius decreases, but they do not differ significantly in a single R compound (Figure 8). These bond distances were gently restrained during the refinement, with a standard deviation of either 0.05 or 0.10 Å. The DFT-optimized metal-oxygen bonds also show the same trend overall (Figure 9). Again, Eu and Ce are anomalous with longer R–O bond distances than the average, and the R–O bonds to the water molecules are longer in the La-terephthalate compound than in the other compounds. However, the DFT R–O bond distances are separated into two distinct groupings of bond distances, with one group of shorter R–O bonds and one group of longer R–O bonds. The long R–O bonds are R–O1, R–O2, R–O7, and R–O8 where O7 and O8 come from the water molecules and O1 and O2 are hydrogen bond acceptors of the carboxyl groups. The short R–O bonds are R–O3, R–O4, R–O5, and R–O6

https://doi.org/10.1017/S0885715622000033 Published online by Cambridge University Press

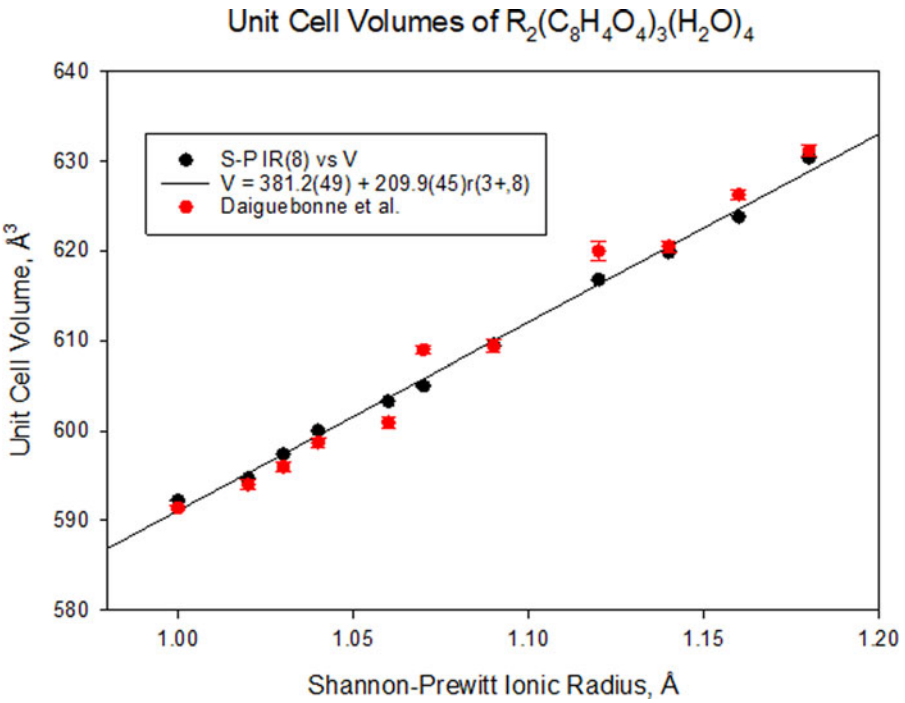

Figure 5. Correlation between the triclinic unit cell volume of $R_2(C_8H_4O_4)_3(H_2O)_4$ with the Shannon-Prewitt ionic radius, both for this study and for Daiguebonne *et al.* (2008).

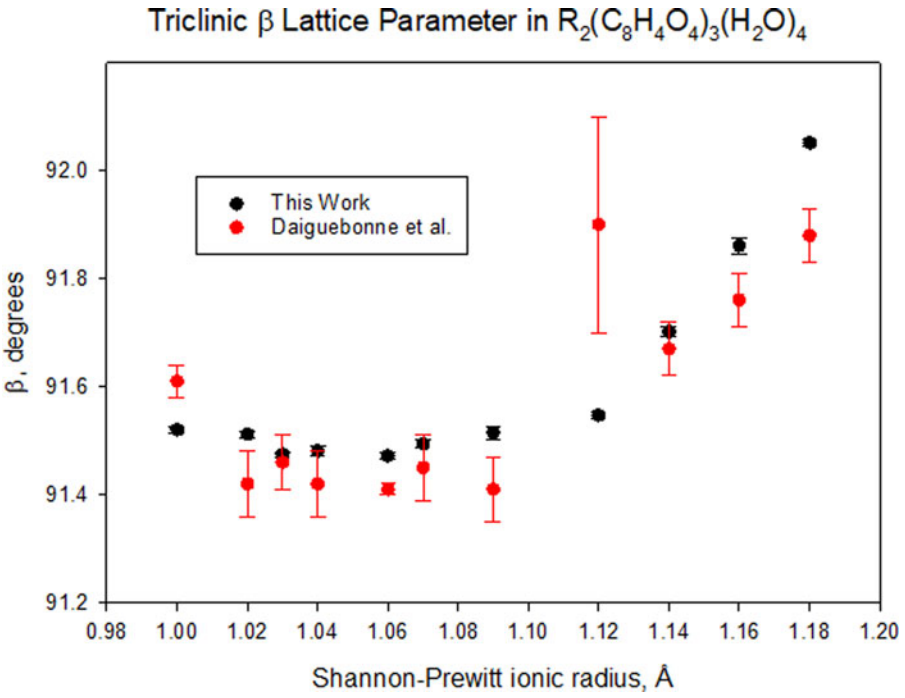

Figure 6. Correlation between the triclinic β angle of $R_2(C_8H_4O_4)_3(H_2O)_4$ with the Shannon-Prewitt ionic radius, both for this study and for Daiguebonne *et al.* (2008).

and are the non-hydrogen bonding carboxyl group. As these bonds are completely unrestrained in the DFT calculations, the difference in the refined and DFT calculated R–O bond distances may indicate that the restraints imposed on the Rietveld-refined structures have a greater effect on the bond distances than would be expected from their weights.

Bond valence sums were calculated from these bond distances (Brown, 2002). The R bond valence sum of these compounds is expected to be 3 as all of the lanthanides are trivalent cations. The average bond valence sum for the experimental structures is 2.91(6), whereas the DFT average is 3.07 (23) (Figure 10). As the bond valence sum is much more

https://doi.org/10.1017/S0885715622000033 Published online by Cambridge University Press

TABLE II. Unusual geometrical features in $R_2(C_8H_4O_4)_3(H_2O)_4$

	Experiment				DFT			
R	Quantity	Observed	Avg(σ)	Z-score	Quantity	Observed	Avg(σ)	Z-score
La	C2–O4	1.138	1.256(10)	11.53				
	O4–C2–O5	123.2	117.7(10)	5.6	O2–C8–O1	121.1	124.8(11)	3.2
	O3–C2–C5	112.4	117.7(10)	5.4				
	O4–C2–C5	123.3	117.7(10)	5.6				
	O1–C8–C10–C12	33.6	Tail of peak ~0°					
Ce	O3–C2–C5	112.0	117.5(16)	3.4	O2–C8–O1	120.6	124.9(8)	5.1
	O4–C2–C5	123.9	117.5(16)	4.1				
	C11–C7–C5	115.6	120.5	3.5				
Pr	C2–O4	1.208	1.252(13)	3.3				
	O4–C2–C5	123.9	117.5(8)	8.0				
	O3–C2–C5	112.0	117.5(8)	6.9				
Nd	C2–O4	1.204	1.246(10)	4.2	C8–O1	1.280	1.246(10)	3.5
					C8–O2	1.287	1.246(10)	4.1
	O3–C2–C5	111.9	117.8(10)	5.7				
	O4–C2–C5	123.9	117.7(11)	5.6				
	C11–C7–C5	111.3	120.5(14)	6.4				
	O1–C8–C10–C12	34.9	Tail of peak ~0°					
Sm	C7–C11	1.445	1.384(17)	3.6				
	O3–C2–O5	112.4	118.0(13)	4.1				
	O4–C2–O5	123.7	118.0(13)	4.1				
	C5–C7–C1	104.9	120.5(14)	11.0				
	C5–C11–C7	134.2	120.5(14)	9.6				
Eu	O4–C2	1.202	1.245(12)	3.6				
	O3–C2–C5	112.8	118.6(13)	3.6				
Gd	C7–C11	1.437	1.384(17)	3.1				
	O3–C2–C5	112.3	118.2(16)	3.8				
	O4–C2–C5	124.2	118.2(16)	3.8				
Tb	C7–C11	1.452	1.384(17)	4.0				
	C5–C7–C11	114.7	120.5(14)	4.1				
Dy	O3–C2–C5	111.9	118.0(12)	4.9				
	O4–C2–C5	124.0	118.0(12)	4.8				
	O1–C8–C10–C12	42.0	Tail of peak ~0°					
Ho								
Er	O4–C8–C1	111.7	116.9(12)	4.4	O2–C8	1.287	1.249(11)	3.4

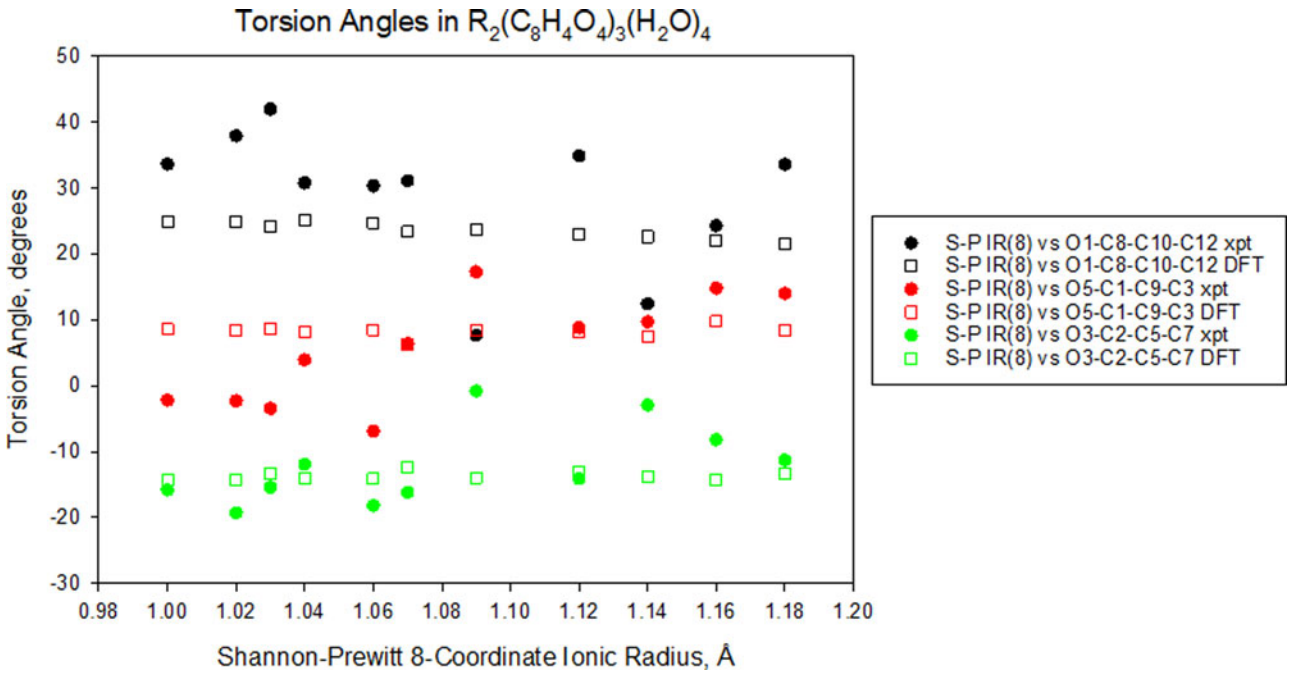

Figure 7. Correlations between the Rietveld-refined and DFT-optimized torsion angles in $R_2(C_8H_4O_4)_3(H_2O)_4$, as a function of the Shannon-Prewitt ionic radius. The experimental values are indicated by filled circles, and the DFT values by open squares.

https://doi.org/10.1017/S0885715622000033 Published online by Cambridge University Press

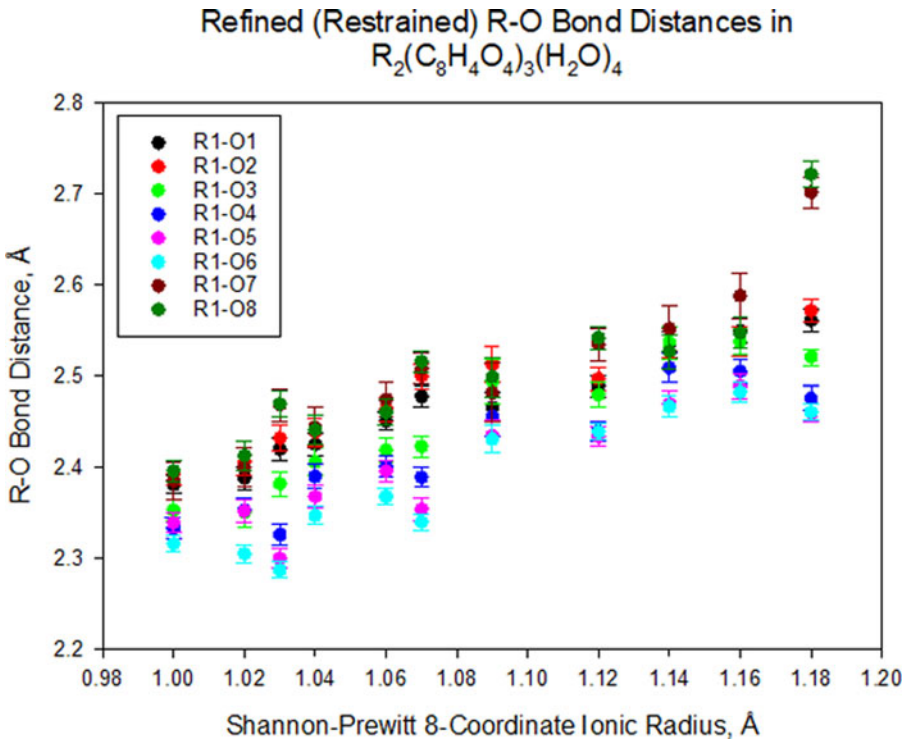

Figure 8. Correlations between the Rietveld-refined (restrained) R–O bond distances in $R_2(C_8H_4O_4)_3(H_2O)_4$, as a function of the Shannon-Prewitt ionic radius.

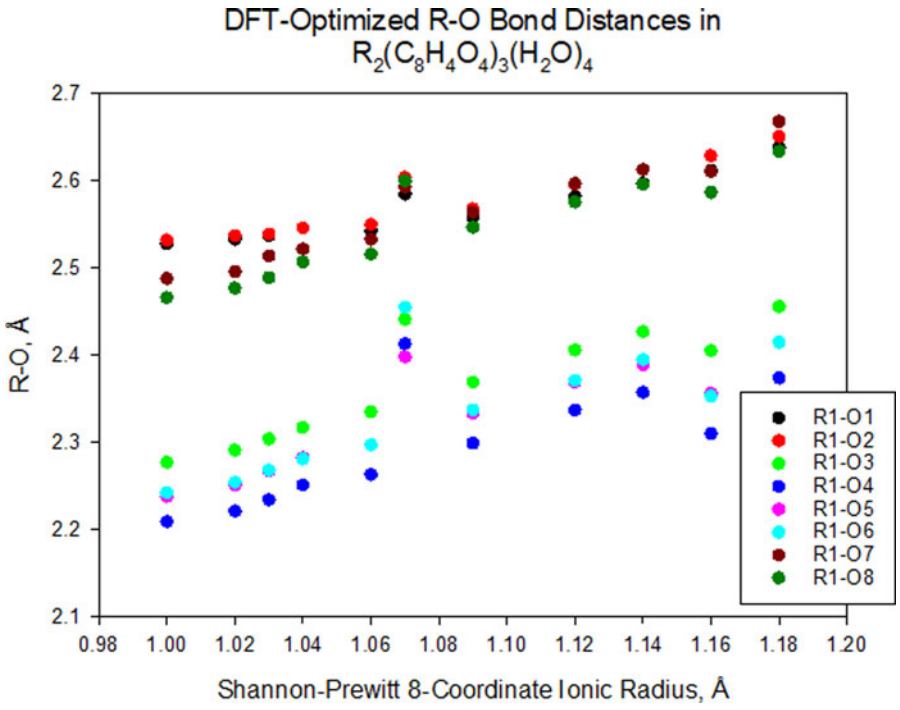

Figure 9. Correlations between the DFT-optimized R–O bond distances in $R_2(C_8H_4O_4)_3(H_2O)_4$, as a function of the Shannon-Prewitt ionic radius.

sensitive to smaller bond distances, it is expected that the DFT calculated average bond valence sum is larger than the experimental average bond valence sum due to the shorter R–O bonds in the DFT structures.

Hydrogen bonds are important in the crystal structures (Figures 11–15). The hydrogen bond analysis is based on the DFT-optimized structures. Each hydrogen atom of each water molecule acts as a donor to the carboxyl oxygen atoms O1 or O2; only one of the carboxyl groups is a hydrogen bond acceptor. The O7–H4 covalent bonds tend to be longer, and thus the H4···O2 distances tend to be shorter. The O–H···O hydrogen bond energies were calculated using the correlation of Rammohan and Kaduk (2018), and are similar.

Analysis of the morphology by the Bravais–Friedel–Donnay–Harker (Bravais, 1866; Friedel, 1907; Donnay and Harker, 1937) model shows we would expect that the lanthanide terephthalate tetrahydrate crystals would be elongated

https://doi.org/10.1017/S0885715622000033 Published online by Cambridge University Press

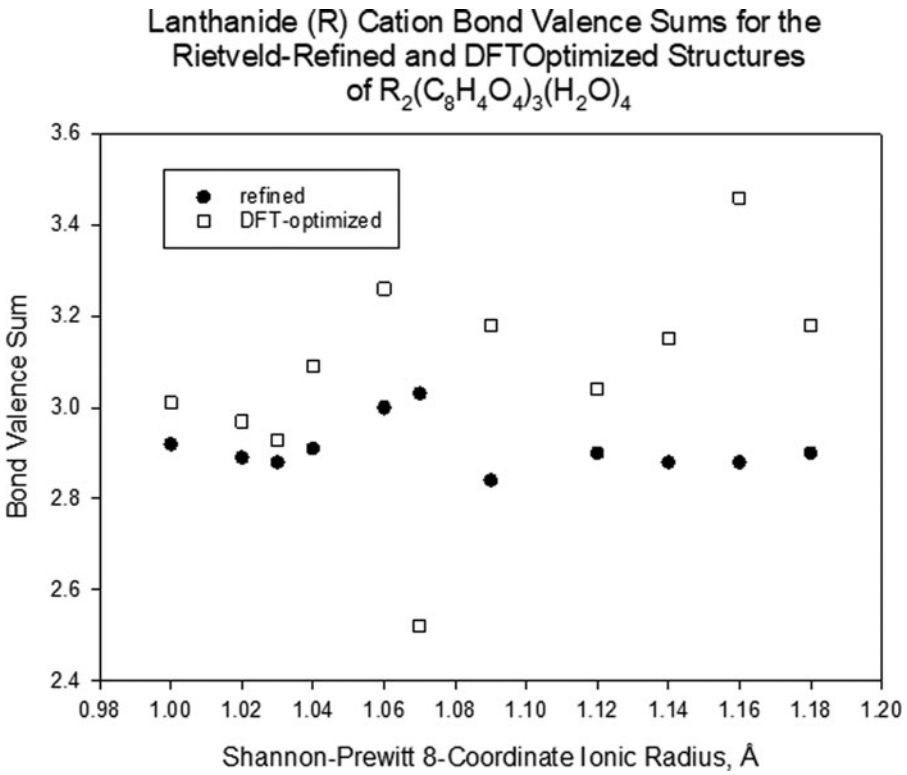

Figure 10. Correlations between the Rietveld-refined and DFT-optimized bond valence sums in $R_2(C_8H_4O_4)_3(H_2O)_4$, as a function of the Shannon-Prewitt ionic radius. The experimental values are indicated by filled circles, and the DFT values by open squares.

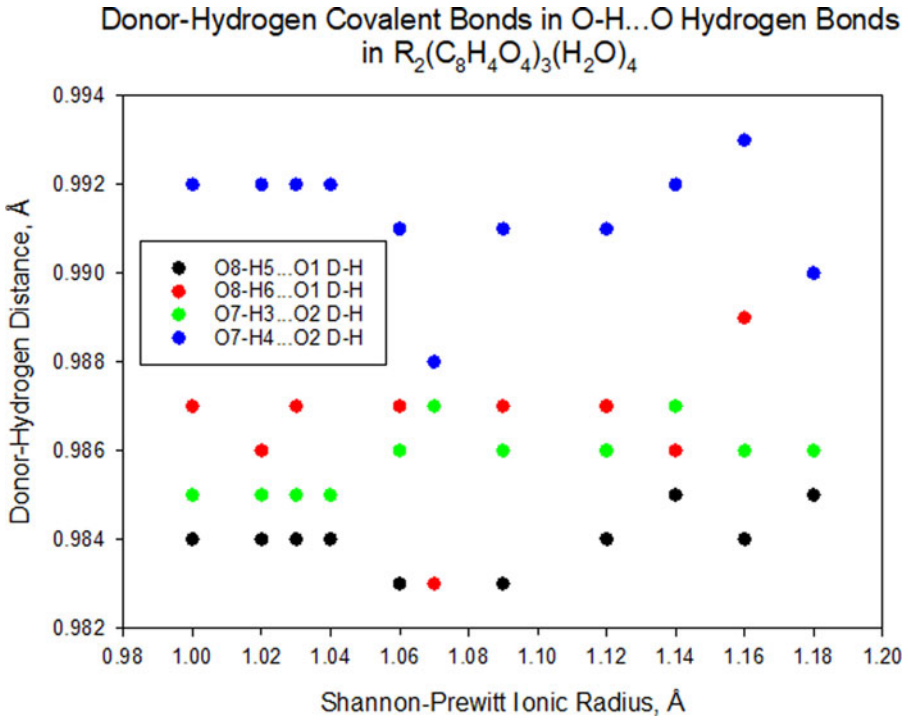

Figure 11. The covalent O–H donor–hydrogen distances in the O–H···O hydrogen bonds in the DFT-optimized structures of $R_2(C_8H_4O_4)_3(H_2O)_4$.

along the *a*-axis; not exactly needle-like, but anisotropic in shape. A second-order spherical harmonic model was included in the refinement of some of these compounds. These refinements produced texture indexes of 1.000, indicating that preferred orientation is not significant in these compounds.

IV. CONCLUSION

We have synthesized 11 isostructural lanthanide terephthalate tetrahydrate compounds $R_2(C_8H_4O_4)_3(H_2O)_4$, R = La–Er, refined their crystal structures using laboratory X-ray powder diffraction data and optimized the structures using density functional techniques. Overall, the lattice parameters

https://doi.org/10.1017/S0885715622000033 Published online by Cambridge University Press

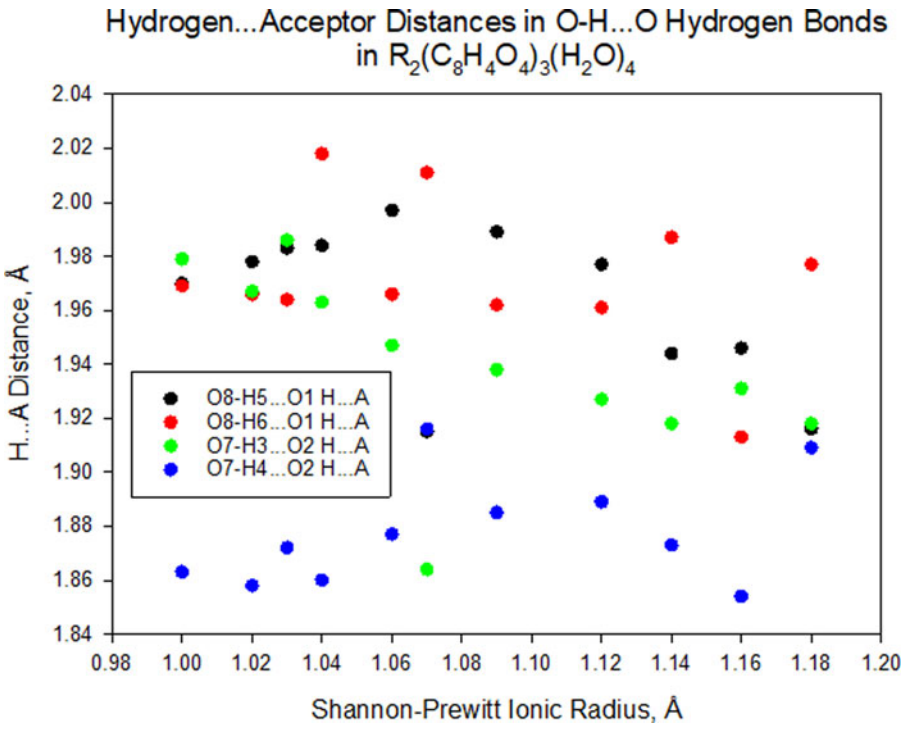

Figure 12. The hydrogen–acceptor distances in the O–H···O hydrogen bonds in the DFT-optimized structures of $R_2(C_8H_4O_4)_3(H_2O)_4$.

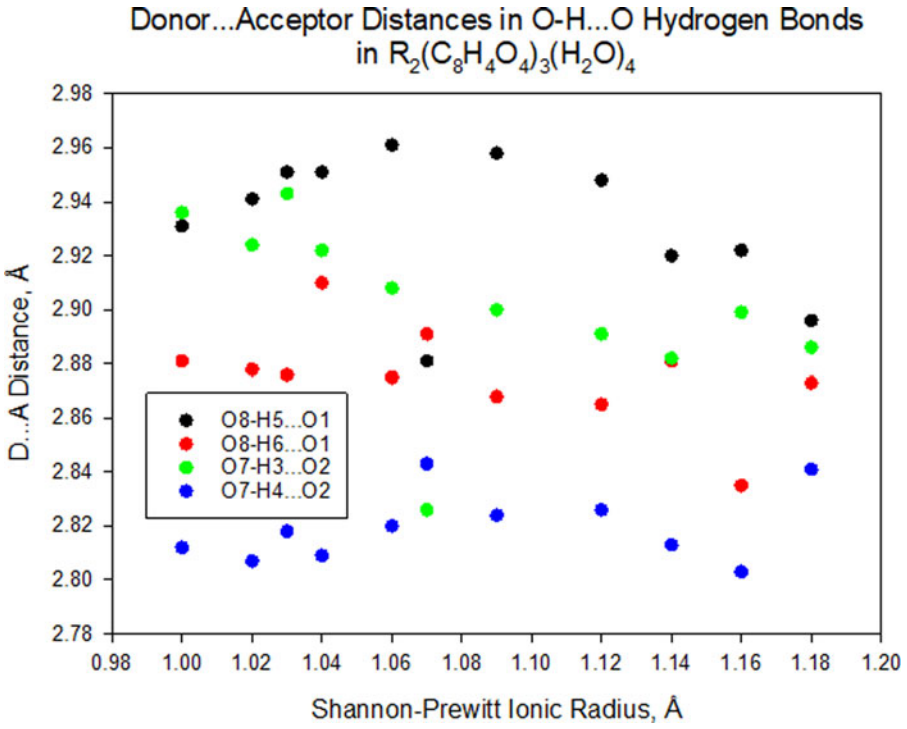

Figure 13. The donor–acceptor distances in the O–H···O hydrogen bonds in the DFT-optimized structures of $R_2(C_8H_4O_4)_3(H_2O)_4$.

and R–O bonds exhibit trends that are expected based on the cation size. The R–O bond distances in the Rietveld-refined structures are similar. However, in the DFT calculated structures, the bond distances break into two distinct groups, longer and shorter R–O bonds. This indicates that the bond distance restraints imposed upon the refined structures may have a greater impact than what is expected due to their weights. The aromatic carboxyl groups were also found to not be completely planar, but it is known that the carboxyl groups can rotate to accommodate hydrogen bonding and

https://doi.org/10.1017/S0885715622000033 Published online by Cambridge University Press

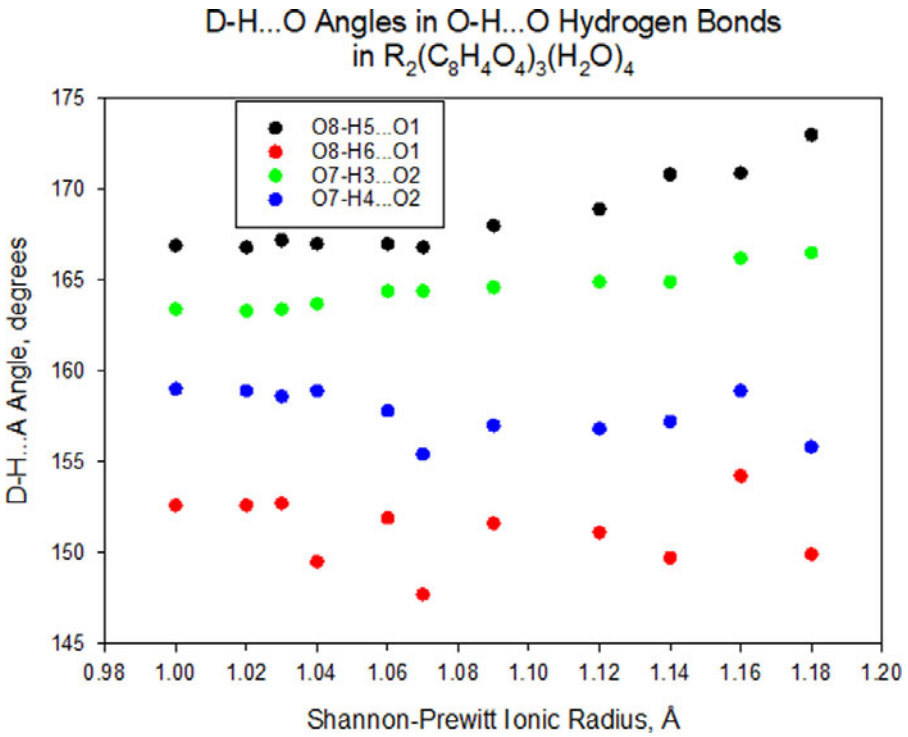

Figure 14. The donor–hydrogen–acceptor angles in the O–H···O hydrogen bonds in the DFT-optimized structures of $R_2(C_8H_4O_4)_3(H_2O)_4$.

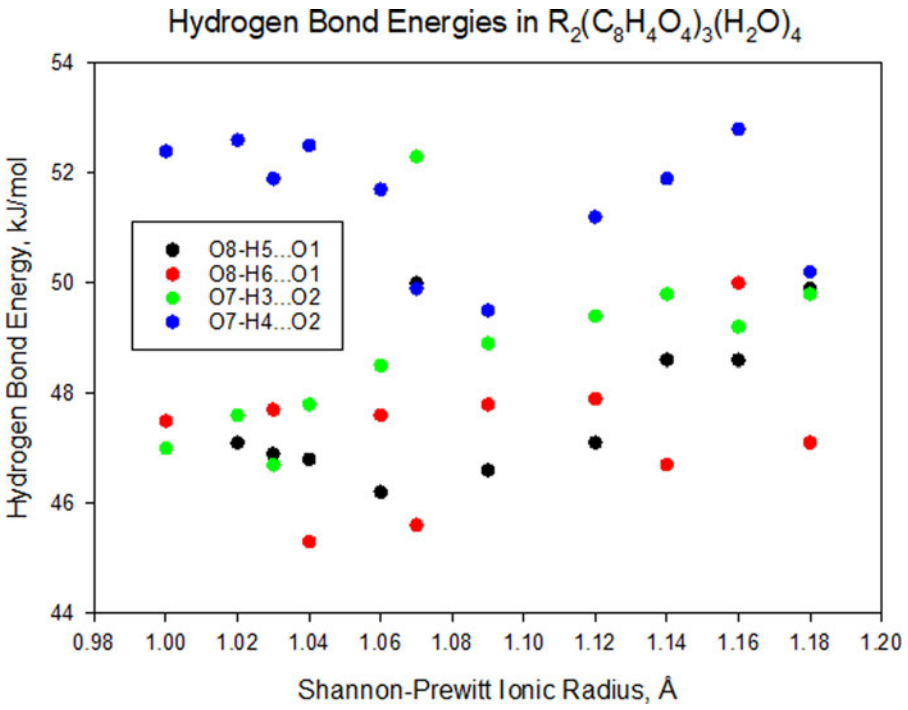

Figure 15. The energies of the O–H···O hydrogen bonds in the DFT-optimized structures of $R_2(C_8H_4O_4)_3(H_2O)_4$.

coordination to the metal. Moreover, all of the water molecules coordinated to the lanthanides act as hydrogen bond donors, but only one of the carboxyl groups of the molecule acts as an acceptor. While four of these structures have been analyzed using single-crystal X-ray diffraction, the agreement between the single crystal and powder structures is good, and the powder patterns for this series of lanthanide terephthalate tetrahydrate can serve as references for future use.

V. DEPOSITED DATA

The supplementary material for this article, which includes the Crystallographic Information Framework (CIF)

https://doi.org/10.1017/S0885715622000033 Published online by Cambridge University Press

files containing the results of the Rietveld refinements (including the raw data) and the DFT geometry optimizations was deposited with the ICDD. The data can be requested at info@icdd.com.

SUPPLEMENTARY MATERIAL

The supplementary material for this article can be found at https://doi.org/10.1017/S0885715622000033.

ACKNOWLEDGEMENTS

The authors would like to thank Dr. Paul F. Brandt and the Irvin A. Koten Research Award (North Central College) for their support of this project.

CONFLICTS OF INTEREST

The authors have no conflicts of interest to declare.

Bravais, A. (**1866**). *Etudes Cristallographiques* (Gauthier Villars, Paris).

Brown, I. D. (**2002**). *The Chemical Bond in Inorganic Chemistry: The Bond Valence Model* (IUCr Monographs on Crystallography 12, Oxford University Press, New York).

Bruno, I. J., Cole, J. C., Kessler, M., Luo, J., Motherwell, W. D. S., Purkis, L. H., Smith, B. R., Taylor, R., Cooper, R. I., Harris, S. E., and Orpen, A. G. (**2004**). "Retrieval of crystallographically-derived molecular geometry information," J. Chem. Inf. Sci. **44**, 2133–2144.

Bushmarinov, I. (**2018**). ICDD Grant-in-Aid; PDF entry 00-069-1206.

Daiguebonne, C., Kerbellec, N., Guillou, O., Bünzil, J.-C., Gumy, F., Catala, L., Mallah, T., Audebrand, N., Gérault, Y., and Bernot, K. (**2008**). "Structural and luminescent properties of micro- and nanosized particles of lanthanide terephthalate coordination polymers," Inorg. Chem. **47**, 3700–3708.

Donnay, J. D. H. and Harker, D. (**1937**). "A new law of crystal morphology extending the law of Bravais," Am. Mineral. **22**, 446–447.

Friedel, G. (**1907**). "Etudes sur la loi de Bravais," Bull. Soc. Fr. Mineral. **30**, 326–455.

Furukawa, H., Cordova, K. E., O'Keeffe, M., and Yaghi, O. M. (**2013**). "The chemistry and applications of metal-organic frameworks," Science **341**, 1230444-1–1230444-12.

Grishko, A. Y., Utochnikova, V. V., Averin, A. A., Mironov, A. V., and Kuzmina, N. P. (**2015**). "Unusual luminescence properties of heterometallic REE terephthalates," Eur. J. Inorg. Chem. **2015**, 1660–1664.

Groom, C. R., Bruno, I. J., Lightfoot, M. P., and Ward, S. C. (**2016**). "The Cambridge Structural Database," Acta Crystallogr. Sect. B: Struct. Sci., Cryst. Eng. Mater. **72**, 171–179.

Kaduk, J. A., Golab, J. T., and Leusen, F. J. J. (**1998**). "The crystal structures of trimellitic anhydride and two of its solvates," Cryst. Eng. **1**, 277–290.

Khudoleeva, V. Y., Utochnikova, V. V., Kalyakina, A. S., Deygen, I. M., Shiryaev, A. A., Marciniak, L., Lebedev, V. A., Roslyakov, I. V., Garshev, A. V., Lepnev, L. S., Schepers, U., Brase, S., and Kuzmina, N. P. (**2017**). "Surface modified $Eu_xLa_{1-x}F_3$ nanoparticles as luminescent biomarkers: still plenty of room at the bottom," Dyes Pigm. **143**, 348–355.

Kozub, A. L., Shick, A. B., Maca, F., Kolorenc, J., and Lichtenstein, A. I. (**2016**). "Electronic structure and magnetism of samarium and neodymium adatoms on free-standing graphene," arXiv:1609,02725v1.

Kresse, G. and Furthmüller, J. (**1996**). "Efficiency of ab-initio total energy calculations for metals and semiconductors using a plane-wave basis set," Comput. Mater. Sci. **6**, 15–50.

Louër, D. and Boultif, A. (**2014**). "Some further considerations in powder diffraction pattern indexing with the dichotomy method," Powder Diffr. **29**, S7–S12.

Macrae, C. F., Sovago, I., Cottrell, S. J., Galek, P. T. A., McCabe, P., Pidcock, E., Platings, M., Shields, G. P., Stevens, J. S., Towler, M., and Wood, P. A. (**2020**). "Mercury 4.0: from visualization to design and prediction," J. Appl. Crystallogr. **53**, 226–235.

Materials Design (**2016**). *MedeA 2.20.4* (Materials Design Inc., Angel Fire, NM).

Rammohan, A. and Kaduk, J. A. (**2018**). "Crystal structures of alkali metal (Group 1) citrate salts," Acta Crystallogr. Sect. B: Cryst. Eng. Mater. **74**, 239–252. doi:10.1107/S2052520618002330.

Serre, C., Millange, F., Marrot, J., and Ferey, G. (**2002**). "Hydrothermal synthesis, structure determination and thermal behavior of new three-dimensional europium terephthalates: MIL-51LT,HT and MIL-52 or $Eu_{2n}(OH)_x(H_2O)_y(O_2C\text{-}C_6H_4\text{-}CO_2)_z$ (n=III, III, II; x=4, 0, 0; y=2, 0, 0; z=1,1,2)," Chem. Mater. **2002**(14), 2409–2415.

Shannon, R. D. and Prewitt, C. T. (**1969**). "Effective ionic radii in oxides and fluorides," Acta Crystallogr. B **25**, 925–946.

Sherif, F. G. (**1970**). "Heavy metal terephthalates," Ind. Eng. Chem. Prod. Res. Develop. **9**, 408–412.

Sykes, R. A., McCabe, P., Allen, F. H., Battle, G. M., Bruno, I. J., and Wood, P. A. (**2011**). "New software for statistical analysis of Cambridge Structural Database data," J. Appl. Crystallogr. **44**, 882–886.

Toby, B. H. and Von Dreele, R. B. (**2013**). "GSAS II: the genesis of a modern open source all purpose crystallography software package," J. Appl. Crystallogr. **46**, 544–549.

Van de Streek, J. and Neumann, M. (**2010**). "Validation of experimental molecular crystal structures with dispersion-corrected density functional theory," Acta Crystallogr. Sect. B: Struct. Sci. **66**, 544–558.

van de Streek, J. and Neumann, M. A. (**2014**). "Validation of molecular crystal structures from powder diffraction data with dispersion-corrected density functional theory (DFT-D)," Acta Crystallogr. Sect. B: Struct. Sci., Cryst. Eng. Mater. **70**(6), 1020–1032.

Wang, Q. and Astruc, D. (**2020**). "State of the art and prospects in metal-organic framework (MOF)-based and MOF-derived nanocatalysis," Chem. Rev. **120**, 1438–1511.

Zehnder, R. A., Renn, R. A., Pippin, E., Zeller, M., Wheeler, K. A., Carr, J. A., Fontaine, N., and McMullen, N. C. (**2011**). "Network dimensionality and ligand flexibility in lanthanide terephthalate hydrates," J. Mol. Struct. **985**, 109–119.

Zhu, M., Fu, W., and Zou, G. (**2012**). "Urothermal synthesis of an unprecedented pillar-layered metal–organic framework," J. Coord. Chem. **65**, 4108–4114.